






Entropy and heat capacity of the transverse momentum distribution for pp collisions at RHIC and LHC energies

D. Rosales Herrera ¹, J. R. Alvarado García ¹, A. Fernández Téllez ¹, J. E. Ramírez ^{2,*} and C. Pajares ³

¹*Facultad de Ciencias Físico Matemáticas, Benemérita Universidad Autónoma de Puebla, Apartado Postal 165, 72000 Puebla, Puebla, Mexico*

²*Centro de Agroecología, Instituto de Ciencias, Benemérita Universidad Autónoma de Puebla, Apartado Postal 165, 72000 Puebla, Puebla, Mexico*

³*Departamento de Física de Partículas and Instituto Galego de Física de Altas Enerxías, Universidad de Santiago de Compostela, E-15782 Santiago de Compostela, Spain*



(Received 11 October 2023; accepted 9 February 2024; published 20 March 2024)

We investigate the transverse momentum distribution (TMD) statistics from three different theoretical approaches. In particular, we explore the framework used for string models, wherein the particle production is given by the Schwinger mechanism. The thermal distribution arises from the Gaussian fluctuations of the string tension. The hard part of the TMD can be reproduced by considering heavy tailed string tension fluctuations, for instance, the Tsallis q -Gaussian function, giving rise to a confluent hypergeometric function that fits the entire experimental TMD data. We also discuss the QCD-based Hagedorn function, another family of fitting functions frequently used to describe the spectrum. We analyze the experimental data of minimum bias pp collisions reported by the BNL Relativistic Heavy Ion Collider (RHIC) and the CERN Large Hadron Collider (LHC) experiments (from $\sqrt{s} = 0.2$ TeV to $\sqrt{s} = 13$ TeV). We extracted the corresponding temperature by studying the behavior of the spectra at low transverse momentum values. For the three approaches, we compute all moments, highlighting the average, variance, and kurtosis. Finally, we compute the Shannon entropy and the heat capacity through the entropy derivative with respect to the temperature. We found that the q -Gaussian string tension fluctuations lead to a monotonically increasing heat capacity as a function of the center-of-mass energy, which is also observed for the Hagedorn fitting function. This behavior is consistent with the experimental observation that the temperature slowly rises with increments of the collision energy.

DOI: [10.1103/PhysRevC.109.034915](https://doi.org/10.1103/PhysRevC.109.034915)

I. INTRODUCTION

The study of high energy ion collisions has been a significant area of research in nuclear and particle physics, providing insights into the properties of strongly interacting matter under extreme conditions [1]. One relevant experimental measurement is the transverse momentum distribution (TMD), which is a *histrogram* built with the transverse momentum (p_T) of the produced charged particles per momentum space unit and contains information on the processes involved in all scales of events, leading to the final state of produced particles [2]. The importance of the TMD necessitates the study of theoretical models and empirical fitting functions that adequately describe part or all the spectrum. Earlier efforts to achieve this assume that the TMD follows an exponential

distribution, where the inverse of the exponential decay is frequently associated with the temperature of the collision system [3,4]. This fitting function reasonably described the experimental data at the lower center-of-mass energies but deviated as experiments reached higher energies, revealing a nonexponential tail [5,6]. This approach is valid when most of the contribution to the spectra comes from soft scattering processes, leading to a soft thermal-like p_T distribution [6–8].

In the early 1980s, Hagedorn introduced a QCD-based fitting function described by a power law of the transverse momentum shifted by a threshold that comes from the elastic scattering momentum scale [9–11]. Interestingly, this proposal reproduced both behaviors of the TMD: thermal and a power law tail at low and high p_T values, respectively. Later, the high energy community presented a new fitting function based on the Tsallis q -exponential function, which generalizes the thermal distribution by introducing a certain nonextensivity degree of the systems formed in high energy collisions [12,13]. However, these fitting functions are shown to be equivalent [14].

On the other hand, for string models, the production of charged particles is described by creating neutral color pairs through the breaking of the strings stretched between the partons. These subsequently decay, producing the observed

*jhony.eredi.ramirez.cancino@cern.ch

Published by the American Physical Society under the terms of the [Creative Commons Attribution 4.0 International](https://creativecommons.org/licenses/by/4.0/) license. Further distribution of this work must maintain attribution to the author(s) and the published article's title, journal citation, and DOI. Funded by SCOAP³.

hadrons [15]. In these cases, the transverse momentum distribution is governed by the Schwinger mechanism [16].

In the latter 1990s, Bialas reconciled this approach with the thermal distribution by considering that the string tension undergoes Gaussian fluctuations with zero average and variance proportional to the string tension [17]. Later, Pajares resumed this idea to incorporate a temperature-like parameter in the color string percolation model, and thus he provided a way to compute the string density from experimental data [18–20]. Recently, in Refs. [21,22], the authors used the original Bialas idea to extend the string tension fluctuations to a heavy tailed distribution. In particular, if the tensions fluctuate according to a q -Gaussian distribution, then the TMD becomes a confluent hypergeometric function that correctly fits the experimental data [21,22].

In this paper, we analyze the TMD data of minimum bias pp collisions reported by the experiments at the BNL Relativistic Heavy Ion Collider (RHIC) and the CERN Large Hadron Collider (LHC) under the three schemes discussed above, namely, the thermal distribution, the Hagedorn, and the confluent hypergeometric fitting functions. In this way, we discuss the thermal temperature estimated in each scenario as a function of the center-of-mass energy. Since each fitting function has a different degree of accuracy in reproducing the spectrum, we compute some statistics to compare them, such as the average of transverse momentum, variance, and kurtosis. Additionally, we compute the Shannon entropy for each fitting function and estimate the heat capacity. The latter determination helps estimate the energy increment necessary to heat the collision systems.

The plan of the paper is as follows. In Sec. II, we comment on different approaches to describe the TMD and their main features. In Sec. III, we show the fits to the TMD of minimum bias pp collisions and give a description of the fit parameters as a function of the center-of-mass energy. In Sec. IV, we compute the moments of the TMD in the approaches discussed in Sec. II. Section V contains our computations of the Shannon entropy and the heat capacity of the analyzed TMD data. Finally, in Sec. VI, we write our final comments, conclusions, and perspectives.

II. THEORETICAL DESCRIPTION OF THE TMD

In this section, we discuss the particularities of the transverse momentum distribution, which can be obtained from different approaches. In particular, we are interested in discussing the cases of the TMD for color string systems and the QCD-based fitting function proposed by Hagedorn. In what follows, the TMD is denoted as dN/dp_T^2 , meaning the invariant yield of produced particles.

A. TMD from the Schwinger mechanism

The Schwinger mechanism explains the generation of particle-antiparticle pairs from the quantum vacuum under the influence of an intense gauge field, which supplies the necessary energy to convert the field's energy into particle neutral pairs. This phenomenon occurs upon the gauge field

surpassing a certain critical intensity, enabling the field's energy to materialize as mass [16].

In terms of the resultant particle dynamics, the Schwinger mechanism describes a p_T -Gaussian distribution of the produced particles TMD. This behavior arises due to the exponential damping linked to the energy barrier imposed by the vacuum [23]. As the transverse momentum magnifies, the likelihood of particle-antiparticle pair production diminishes exponentially. Initially, the Schwinger mechanism was conceived to explain the emergence of electron-positron pairs within a potent electromagnetic field [16]; then, it was broadened to the creation of quark-antiquark and quark-quark-antiquark-antiquark pairs within the framework of QCD. These pairs promptly amalgamate into color-neutral hadrons, yielding the transverse momentum distribution of the observed particles.

Taking these ideas into consideration, the probability of observing a produced hadron with momentum p_T is proportional to [16,24]

$$\frac{dN}{dp_T^2} \sim e^{-\pi p_T^2/x^2}, \quad (1)$$

where x^2 is the string tension associated with the energy supplied to the vacuum in the context of QCD color string models.

B. Thermal TMD

As we commented in Sec. II A, the Schwinger mechanism has been adequately adapted to describe the production of charged particles in high energy physics and relates the energy supplied to the vacuum for the pair creation with the string tension in QCD [25]. First, it was proposed that the tension of the color string was taken as a constant. Later, Bialas introduced the string tension fluctuations based on a stochastic QCD-vacuum approach [17]. In this way, if the tension of the strings is considered as a random variable described by a probability density function $P(x)$, then the appropriate computation of the spectrum should consider these fluctuations, which can be done by performing the following convolution:

$$\frac{dN}{dp_T^2} \propto \int_0^\infty e^{-\pi p_T^2/x^2} P(x) dx. \quad (2)$$

Assuming that the string tension fluctuations are described by a Gaussian distribution, the Schwinger mechanism becomes

$$\frac{dN}{dp_T^2} \propto e^{-p_T/T_{\text{th}}}, \quad (3)$$

where $T_{\text{th}} = \langle p_T \rangle / 2$ [17]. Equation (3) can be interpreted as a *thermal distribution* because it is similar to the Boltzmann distribution. T_{th} can be understood as the temperature linked to the TMD, computed over the ensemble of collision events occurring under identical conditions [26].

C. Soft and hard scales of the TMD from string tension fluctuations

In Sec. II B, we discussed the origin of the TMD thermal distribution from the fluctuations of the string tension. This

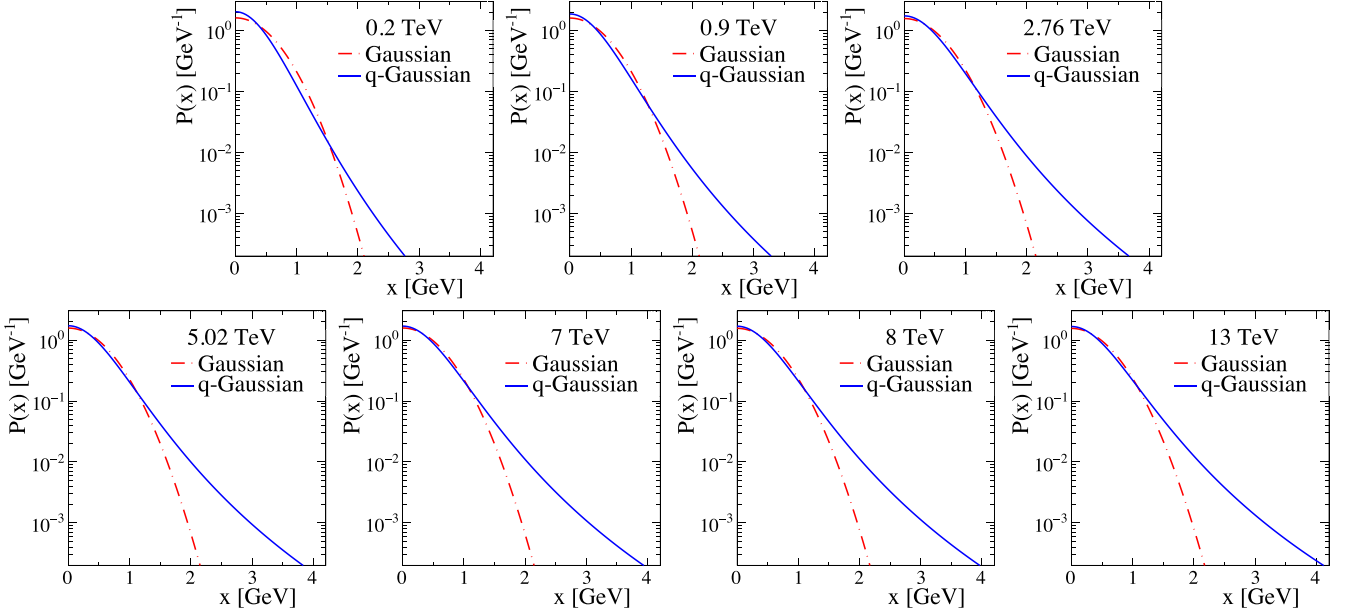


FIG. 1. Gaussian and q -Gaussian string tension fluctuations for pp collisions at different center-of-mass energies. The tail of the q -Gaussian distribution becomes less tilted as the center-of-mass energy increases, which means that the probability of observing a string with a higher tension rises.

approach reproduces the thermal behavior of the TMD but fails to describe the power-like law of the TMD tail at high p_T values.

Recently, it was shown that the spectrum can be adequately described by replacing the Gaussian fluctuations of the string tension with a q -Gaussian distribution [21,22], which reads

$$P(x) = \mathcal{N} \left(1 + \frac{(q-1)x^2}{2\sigma^2} \right)^{\frac{1}{1-q}}, \quad (4)$$

with zero mean value, scale parameter σ , and \mathcal{N} being the normalization constant. To allow variations in the string tension across a range from zero to infinity, it is necessary that the parameter q lies between 1 and 3 [22,27,28]. In general, this q -Gaussian distribution is heavy tailed, which means that, in the collision system the probability of observing a string with higher tensions is greater than in the Gaussian case, as we depict in Fig. 1 for pp collisions at different center-of-mass energies (further analyzed below).

Following the same procedure as in Sec. II B, and by introducing the variable $t = 2\sigma^2/[(q-1)x^2]$, the convolution (2) now reads

$$\frac{dN}{dp_T^2} \propto \int_0^\infty e^{-\frac{\pi p_T^2 (q-1)}{2\sigma^2} t} t^{\frac{1}{q-1} - \frac{3}{2}} (1+t)^{\frac{1}{1-q}} dt. \quad (5)$$

By comparing Eq. (5) with the confluent hypergeometric function defined as

$$U(a, b, z) = \frac{1}{\Gamma(a)} \int_0^\infty e^{-zt} t^{a-1} (1+t)^{b-a-1} dt, \quad (6)$$

we identify

$$a = \frac{1}{q-1} - \frac{1}{2}, \quad b = 1/2, \quad \text{and} \quad z = \pi p_T^2 \frac{q-1}{2\sigma^2}. \quad (7)$$

Therefore, the spectrum (5) becomes

$$\frac{dN}{dp_T^2} \propto \Gamma\left(\frac{1}{q-1}\right) U\left(\frac{1}{q-1} - \frac{1}{2}, \frac{1}{2}, \pi p_T^2 \frac{q-1}{2\sigma^2}\right). \quad (8)$$

In particular, Eq. (8) reproduces the exponential decay at low p_T region, reaching the asymptotic behavior

$$\frac{dN}{dp_T^2} \sim e^{-p_T/T_U}, \quad (9)$$

where the thermal temperature T_U is defined as

$$T_U = \sigma \frac{\Gamma\left(\frac{1}{q-1} - \frac{1}{2}\right)}{\sqrt{2\pi(q-1)}\Gamma\left(\frac{1}{q-1}\right)}. \quad (10)$$

On the other hand, for high p_T values, the TMD (8) behaves as a power law in p_T^2

$$\frac{dN}{dp_T^2} \sim \frac{\Gamma\left(\frac{1}{q-1}\right)}{\sqrt{\pi}} \left(\frac{\pi p_T^2 (q-1)}{2\sigma^2}\right)^{\frac{1}{2} - \frac{1}{q-1}}, \quad (11)$$

from where we define the hard scale

$$T_{H,U} = \sigma \sqrt{\frac{2}{\pi(q-1)}} \left(\frac{\sqrt{\pi}}{\Gamma\left(\frac{1}{q-1}\right)}\right)^{\frac{q-1}{q-3}}. \quad (12)$$

Note that the soft (10) and hard (12) scales only depend on the q -Gaussian parameters.

It is worth mentioning that, from (9) and (11), the U fitting function reproduces the well-known soft and hard behaviors of the TMD [29].

D. Hagedorn-like fitting functions

A different description of the TMD comes from a formula inspired by QCD. The Hagedorn function is concerned with

describing the hard part of the spectrum at high p_T values. This fitting function is given by

$$\frac{dN}{dp_T^2} \propto \left(\frac{p_0}{p_0 + p_T} \right)^m. \quad (13)$$

It is straightforward to show that the latter is a Tsallis q -exponential function by doing the following parametrization: $m = 1/(q_e - 1)$ and $p_0 = \lambda/(q_e - 1)$. Therefore, the Hagedorn spectrum becomes

$$\frac{dN}{dp_T^2} \propto \left(1 + \frac{p_T}{p_0} \right)^{-m} = \left(1 + (q_e - 1) \frac{p_T}{\lambda} \right)^{\frac{1}{1-q_e}}, \quad (14)$$

where we have added the subscript e to q_e in order to avoid confusion with the q parameter of the string tension fluctuations (4).

Other authors consider a fitting function similar to (14), where the exponent m is replaced with $q'_e/(q'_e - 1)$. They use as variable the transverse mass $m_T^2 = p_T^2 + m_0^2$, where m_0 is the mass of the produced particle [30–33]. The Tsallis distribution has been used to fit the TMD by experiments such as those of the STAR Collaboration [34] at RHIC and the ALICE [35] and CMS [36] Collaborations at LHC. It is convenient to replace m_T with p_T . In this case, the TMD is given by

$$\frac{dN}{dp_T^2} \propto \left(1 + (q'_e - 1) \frac{p_T}{\tau} \right)^{\frac{q'_e}{1-q'_e}}, \quad (15)$$

which also can be expressed as a Tsallis q -exponential if we replace q_e and λ with $2 - 1/q'_e$ and τ/q'_e , respectively. Notice that Eqs. (13), (14), and (15) are equivalent, and they must describe the same behaviors of the TMD at low and high p_T values. For instance, in the limit of low p_T

$$\frac{dN}{dp_T^2} \propto 1 - \frac{p_T}{T_{\text{Hag}}} + \mathcal{O}(p_T^2) \sim e^{-p_T/T_{\text{Hag}}}, \quad (16)$$

where T_{Hag} is the slope of the spectrum at low p_T , which is given by p_0/m , λ , and τ/q'_e for (13), (14), and (15), respectively. Nevertheless, it is worth mentioning that, for the cases of the q -exponential (15), τ is usually used as a temperature parameter [30,32,33]. However, this parameter does not consider the complete slope in the argument of the thermal distribution, leading to an overestimation of thermal temperature when $q'_e > 1$, as observed in the cases discussed in this paper.

On the other hand, at high values of p_T , it is found that

$$\frac{dN}{dp_T^2} \propto \left(\frac{p_T}{T_{H,\text{Hag}}} \right)^\alpha, \quad (17)$$

where $T_{H,\text{Hag}}$ is identified in (17) as p_0 [11], $\lambda/(q_e - 1)$, and $\tau/(q'_e - 1)$ for (13), (14), and (15), respectively. Usually, $T_{H,\text{Hag}}$ is referred to as the hard scale of the TMD [37–41]. Moreover, the α parameter corresponds to the exponent of the TMD fitting function of each case.

III. EXPERIMENTAL TMD DATA ANALYSIS

We analyze the experimental transverse momentum spectra of charged particles of minimum bias pp collisions at different center-of-mass energies. By using Eqs. (3), (8), and

TABLE I. p_T ranges for the thermal fit and their corresponding temperatures.

\sqrt{s} (TeV)	$p_{T,\text{min}}$ (GeV)	$p_{T,\text{max}}$ (GeV)	T_{th} (GeV)
0.20	0.40	0.90	0.197(31)
0.90	0.15	0.70	0.199(10)
2.76	0.15	0.50	0.202(20)
5.02	0.15	0.60	0.203(13)
7.00	0.15	0.55	0.202(16)
8.00	0.15	0.60	0.204(14)
13.00	0.15	0.60	0.205(13)

(13), we fit the experimental data reported on Refs. [42–44] using the ROOT 6 software. The fits were performed by using different p_T ranges. For instance, we adjust the p_T range for the thermal fits, finding the minimization of χ^2 (see Table I). However, for the Hagedorn and U functions, the fit was done for the entire p_T range reported by the experiments [42–44]. In all cases, the value of the quotient χ^2/NDF does not exceed 1 for the fits performed to the TMD data. Nevertheless, $\chi^2/\text{NDF} \gg 1$ in the case of the thermal fits extrapolated to the entire range of p_T . This means that the three functions can provide a good description of the experimental data in the appropriate p_T range. As seen in Fig. 2, the thermal fit reproduces only the low p_T region. Meanwhile, the Hagedorn function was proposed to describe the high p_T region of the spectrum ($0.3 < p_T < 10$ GeV [11]) but is capable of reproducing the complete range of experimental data. Finally, the confluent hypergeometric function successfully describes the behavior of the whole TMD for the data sets.

It is found that the q -Gaussian parameters rise as the center-of-mass energy increases. We propose the following scaling laws to describe these behaviors:

$$q(\sqrt{s}) = a_q \left(\sqrt{\frac{s}{s_0}} \right)^{c_q}, \quad (18a)$$

$$\sigma(\sqrt{s}) = a_\sigma \left(\sqrt{\frac{s}{s_0}} \right)^{c_\sigma}, \quad (18b)$$

with $\sqrt{s_0} = 1$ GeV, $a_q = 1.253(3)$, $c_q = 0.0154(14)$, $a_\sigma = 0.388(8)$ GeV, and $c_\sigma = 0.037(11)$. In Fig. 3 we plot the q and σ dependence on \sqrt{s} described by Eqs. (18).

For the Hagedorn function, the fitting parameters m and p_0 are described by

$$m(\sqrt{s}) = a_m \left(\sqrt{\frac{s}{s_0}} \right)^{c_m}, \quad (19a)$$

$$p_0(\sqrt{s}) = a_{p_0} \left(\sqrt{\frac{s}{s_0}} \right)^{c_{p_0}}, \quad (19b)$$

with $a_m = 8.45(17)$, $c_m = -0.082(11)$, $a_{p_0} = 1.22(5)$ GeV, and $c_{p_0} = -0.03(3)$. Figure 4 shows the Hagedorn parameters' dependence on \sqrt{s} . The parameter $q_e = (1 + m)/m$ is also shown in Fig. 4(a) in the y axis on the right side.

We recall that the three different approaches to analyzing the TMD provide their estimation of the thermal temperature. We found that T_{th} , T_U , and T_{Hag} scale with the center-of-mass

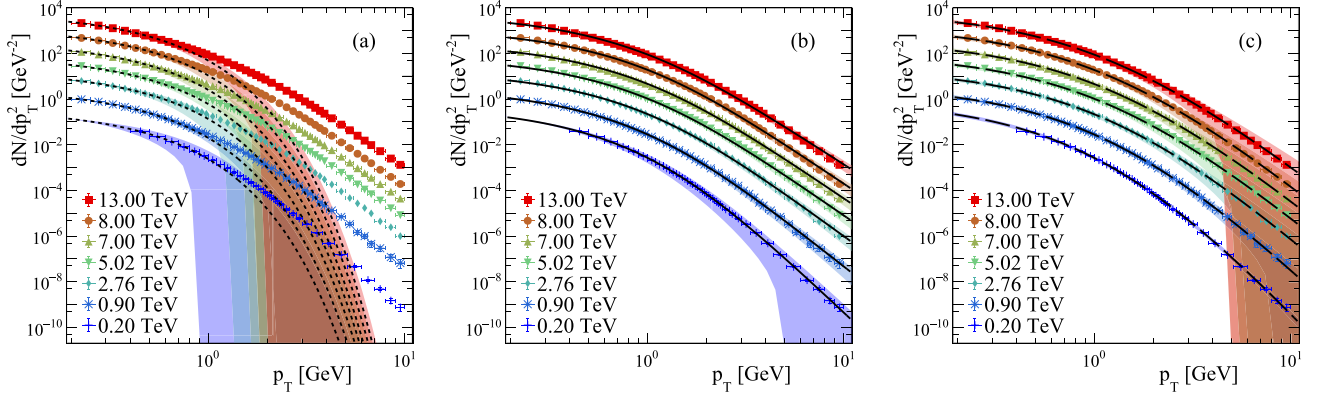


FIG. 2. Fits (lines) to the experimental data (figures) for minimum bias pp collisions at different center-of-mass energies by using (a) the thermal distribution, (b) the hypergeometric confluent U function, and (c) the Hagedorn function. Shaded regions correspond to the 95% uncertainty propagation.

energy as [22]

$$T(\sqrt{s}) = a_T \left(\sqrt{\frac{s}{s_0}} \right)^{c_T}. \quad (20)$$

The obtained parameters of Eq. (20) for the three approaches are shown in Table II, and the temperatures are plotted in Fig. 5.

We recall that the temperature parameter is given by the TMD behavior at low p_T . The experimental TMD data exhibit a thermal behavior at low p_T for identified species of produced particles, including the Higgs boson [21]. For higher masses, higher temperature values are expected. The collisions may also produce heavy resonances which decay into lower mass particles, enhancing the low p_T spectrum, but they cannot be considered as formerly produced by the fragmentation of color string clusters. Notice that the parameters q and m control the tail of the TMD, exhibiting a monotonic behavior with the center-of-mass energy, as shown in Figs. 3(a) and 4(a). Similar behaviors are expected as a function of the multiplicity. Additionally, in the heavy-tailed string tension fluctuations approach, the high p_T particle production can be considered as rare events, including jets. This information is implicitly incorporated in the tail of the q -Gaussian fluctua-

tions. Nevertheless, this approach is not able to distinguish the longitudinal and transverse jet structure.

IV. MOMENTS OF THE TMD

We compute the n th moment of the transverse momentum spectra in the standard form

$$\langle \mathcal{P}_T^n \rangle = \frac{\int_0^\infty p_T^n \text{TMD} dp_T}{\int_0^\infty \text{TMD} dp_T}, \quad (21)$$

for all the fitting functions discussed in Sec. II. Here, we have introduced the notation $\langle \mathcal{P}_T^n \rangle$ to avoid confusion with the computation of the moments reported by the high energy physics community. In those cases, the TMD must be integrated by considering the differential contributions of the longitudinal momentum component [11,38]. Then

$$\langle p_T^n \rangle = \frac{\int p_T^n \text{TMD} 2\pi p_T dp_T}{\int \text{TMD} 2\pi p_T dp_T} = \frac{\langle \mathcal{P}_T^{n+1} \rangle}{\langle \mathcal{P}_T \rangle}. \quad (22)$$

This latter definition is also equivalent to considering p_T^2 as the random variable.

The calculation of (21) is immediate for the thermal distribution, which gives $\langle \mathcal{P}_T^n \rangle_{\text{exp}} = n! T^n$.

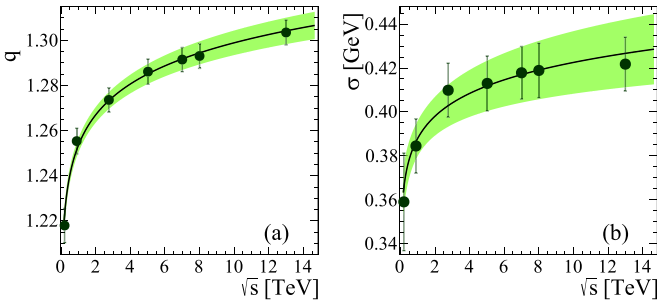


FIG. 3. Values of the parameters (a) q and (b) σ obtained from the confluent hypergeometric U fits as a function of center-of-mass energy for minimum bias pp collisions. The scaling law dependences (18) are shown in solid lines. Shaded regions correspond to the uncertainty propagation.

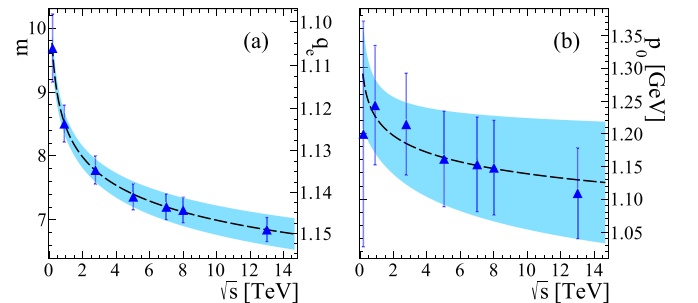


FIG. 4. Parameters (a) m and (b) p_0 obtained from Hagedorn fits (13) to minimum bias pp collisions data as a function of the center-of-mass energy. Dashed lines are the parameters described by (19). The shaded regions correspond to the propagation of uncertainty.

TABLE II. Fit parameter values of the temperature behavior as a function of the center-of-mass energy (20) for each model.

Model	a_T (GeV)	c_T
Thermal	0.199(8)	0.011(24)
Hypergeometric U	0.172(4)	0.046(11)
Hagedorn	0.145(7)	0.051(28)

Let us explain the computation of $\langle \mathcal{P}_T^n \rangle$ for the Hagedorn and confluent hypergeometric U functions in detail. In both cases, we define the auxiliary function

$$I_n = \int_0^\infty p_T^n \text{TMD} dp_T. \quad (23)$$

In this way, $\langle \mathcal{P}_T^n \rangle = I_n/I_0$. For the Hagedorn function (13), we found

$$\begin{aligned} I_n &= \int_0^\infty p_T^n \left(1 + \frac{p_T}{p_0}\right)^{-m} dp_T \\ &= p_0^{n+1} \int_0^1 y^{m-n-2} (1-y)^n dy \\ &= p_0^{n+1} B(m-n-1, n+1), \end{aligned}$$

where B is the beta function, which is well defined for $m > n+1$. Therefore

$$\langle \mathcal{P}_T^n \rangle_{\text{Hag}} = (m-1)p_0^n B(m-n-1, n+1). \quad (24)$$

Similarly, for the U function, we need to compute the integral

$$I_n = \int_0^\infty p_T^n U(a, b, z) dp_T,$$

where a , b , and z correspond to Eq. (7). By following the definition of the confluent hypergeometric function (6), we

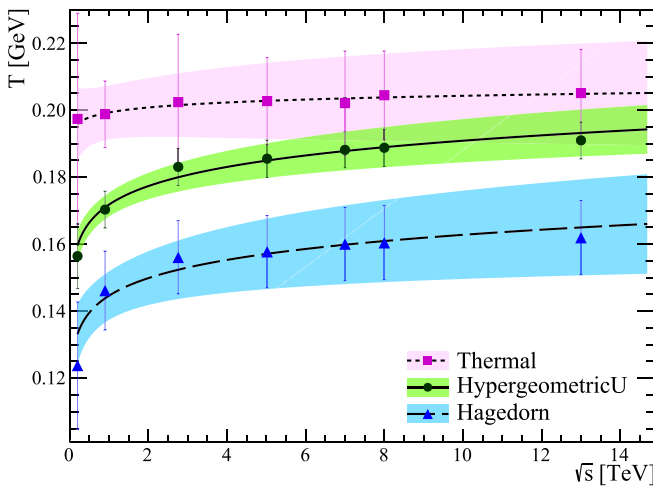


FIG. 5. Temperature extracted from (squares) thermal, (circles) confluent hypergeometric U , and (triangles) Hagedorn fitting functions. Lines are the trend of the (dotted) T_{th} , (solid) T_U , and (dashed) T_{Hag} described by Eq. (20). Shaded regions correspond to the uncertainty propagation.

rewrite I_n as

$$I_n = \int_0^\infty \int_0^\infty p_T^n e^{-\pi p_T^2 \frac{q-1}{2\sigma^2} t} t^{a-1} (1+t)^{b-a-1} dt dp_T. \quad (25)$$

To simplify notation, we omitted writing the factor $1/\Gamma(a)$, which appears in the denominator and numerator of Eq. (21). Note that the integral over p_T in Eq. (25) is a Gaussian integral,

$$\begin{aligned} &\int_0^\infty p_T^n e^{-\pi p_T^2 \frac{q-1}{2\sigma^2} t} dp_T \\ &= \frac{1}{2} \Gamma\left(\frac{n+1}{2}\right) \left(\pi \frac{q-1}{2\sigma^2}\right)^{-(n+1)/2} t^{-(n+1)/2}. \end{aligned} \quad (26)$$

By plugging this into Eq. (25) and performing the change of variable $y = (t+1)^{-1}$, the remaining integral becomes

$$\begin{aligned} &\int_0^1 (1-y)^{a-1-(n+1)/2} y^{-(b-(n+1)/2)} dy \\ &= B\left(1 - \left(b - \frac{n+1}{2}\right), a - \frac{n+1}{2}\right). \end{aligned} \quad (27)$$

Finally, the I_n integrals are given by

$$\begin{aligned} I_n &= \frac{1}{2} \Gamma\left(\frac{n+1}{2}\right) \left(\pi \frac{q-1}{2\sigma^2}\right)^{-(n+1)/2} \\ &\quad \times B\left(\frac{n+2}{2}, \frac{1}{q-1} - \frac{n+2}{2}\right), \end{aligned} \quad (28)$$

which are well defined if $q < (4+n)/(2+n)$. So, the moments of the distribution are expressed as

$$\begin{aligned} \langle \mathcal{P}_T^n \rangle_U &= \frac{1}{\sqrt{\pi}} \Gamma\left(\frac{n+1}{2}\right) \left(\frac{2-q}{q-1}\right) \left(\frac{2\sigma^2}{\pi(q-1)}\right)^{n/2} \\ &\quad \times B\left(\frac{n+2}{2}, \frac{1}{q-1} - \frac{n+2}{2}\right). \end{aligned} \quad (29)$$

It is worth mentioning that some experiments report the TMD without the functional normalization by dividing by p_T . In those cases, the function describing the transverse momentum spectra is $p_T(dN/dp_T^2)$, and the moments of the distribution are calculated as discussed above. Notice that the moments (22) can also be expressed in terms of the I_n integrals as I_{n+1}/I_1 . Moreover, the ratio $\langle \mathcal{P}_T^n \rangle / \langle p_T^n \rangle$ is given by

$$\frac{\langle \mathcal{P}_T^n \rangle_{\text{th}}}{\langle p_T^n \rangle_{\text{th}}} = \frac{1}{n+1}, \quad (30a)$$

$$\frac{\langle \mathcal{P}_T^n \rangle_{\text{Hag}}}{\langle p_T^n \rangle_{\text{Hag}}} = \frac{m-n-2}{(n+1)(m-2)}, \quad (30b)$$

$$\frac{\langle \mathcal{P}_T^n \rangle_U}{\langle p_T^n \rangle_U} = \frac{B\left(\frac{1}{q-1} - \frac{3}{2}, \frac{1}{q-1} - \frac{n+2}{2}\right)}{(n+1)B\left(\frac{1}{q-1} - 1, \frac{1}{q-1} - \frac{n+3}{2}\right)}, \quad (30c)$$

for the thermal, Hagedorn, and confluent hypergeometric U functions, respectively. Nevertheless, in what follows, we will continue to discuss the computation of observables considering p_T as the random variable.

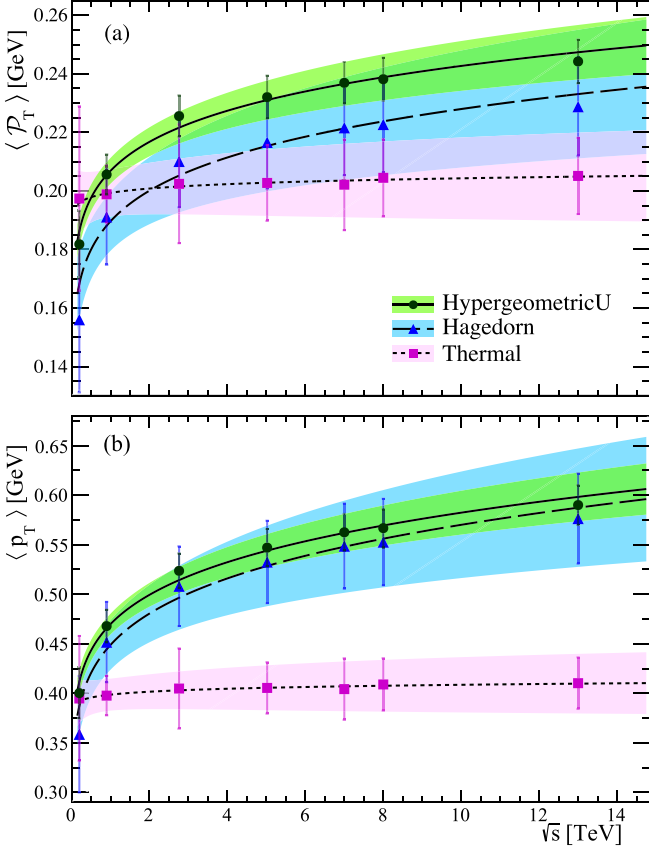


FIG. 6. (a) $\langle \mathcal{P}_T \rangle$ and (b) $\langle p_T \rangle$ as a function of the center-of-mass energy for pp collisions for the three different fitting functions with their corresponding parameter dependence. Lines, figures, and colors are the same as in Fig. 5.

A. Average of transverse momentum

The first moments of p_T of the three different approaches are given by

$$\langle \mathcal{P}_T \rangle_{\text{th}} = T_{\text{th}}, \quad (31a)$$

$$\langle \mathcal{P}_T \rangle_{\text{Hag}} = \frac{m}{m-2} T_{\text{Hag}}, \quad (31b)$$

$$\langle \mathcal{P}_T \rangle_U = \frac{4-2q}{5-3q} T_U. \quad (31c)$$

The transverse momentum averages are

$$\langle p_T \rangle_{\text{th}} = 2T_{\text{th}}, \quad (32a)$$

$$\langle p_T \rangle_{\text{Hag}} = \frac{2m}{m-3} T_{\text{Hag}}, \quad (32b)$$

$$\langle p_T \rangle_U = \frac{(q-1)(3q-5)}{(2-q)(2q-3)} \left(\frac{\Gamma(\frac{1}{q-1})}{\Gamma(\frac{1}{q-1} - \frac{1}{2})} \right)^2 T_U. \quad (32c)$$

We recall that the fit parameters q , σ , m , p_0 , and T_{th} exhibit a particular dependence with the center-of-mass energy for the case of minimum bias pp collisions. This behavior can be incorporated into the average of p_T by plugging Eqs. (18), (19), and (20) into Eqs. (31), and (30) for $n=1$. Figure 6 shows the behaviors of $\langle \mathcal{P}_T \rangle$ and $\langle p_T \rangle$ as a function of the center-of-mass energy of minimum bias pp collisions for the

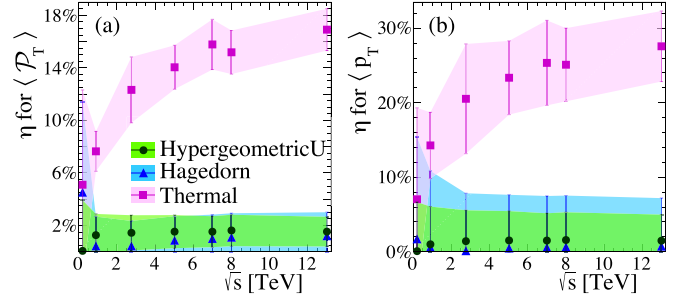


FIG. 7. Absolute percentile deviations of (a) $\langle \mathcal{P}_T \rangle$ and (b) $\langle p_T \rangle$ for the confluent hypergeometric U (circles), Hagedorn (triangles) and thermal (squares) fitting functions. Figures and colors are the same as in Fig. 5.

three different approaches with their corresponding estimations discussed above.

It is worth mentioning that the average of p_T is proportional to the thermal temperature in the three approaches, given by simple combinations of q and m for the U and Hagedorn functions, respectively. These parameters are the exponents that modulate the hard part of the TMD. Equations (32b) and (32c) lead to an enhancement of the $\langle p_T \rangle$ when compared with the thermal function, as seen in Fig. 6, but they recover Eq. (32a) in the limit $q \rightarrow 1$ and $m \rightarrow \infty$.

Additionally, we can compare the average of the transverse momentum statistics computed directly from the experimental TMD data. Thus, the n -moment is calculated as discussed above, but now we compute the I_n integrals as follows:

$$I_n^{\text{hist}} = \sum_k p_{T_k}^n \text{TMD}_k \Delta p_{T_k}, \quad (33)$$

where k is the bin number, $p_{T_k}^n$ is the conservative p_T value of the k bin, TMD_k is the TMD value reported for the k bin, and Δp_{T_k} is the bin width. We also added the superscript “hist” to differentiate the I_n integrals computed from the TMD histogram. Moreover, to compare the predictions of the fitting function, we define the absolute percentage of deviation as

$$\eta = \frac{|\langle \mathcal{P}_T \rangle^{\text{hist}} - \langle \mathcal{P}_T \rangle^{\text{trunc}}|}{\langle \mathcal{P}_T \rangle^{\text{hist}}}, \quad (34)$$

where $\langle \mathcal{P}_T \rangle^{\text{hist}} = I_1^{\text{hist}}/I_0^{\text{hist}}$, and

$$\langle \mathcal{P}_T \rangle^{\text{trunc}} = \frac{1}{I_0^{\text{hist}}} \int_{\mathcal{R}} p_T \text{TMD} dp_T, \quad (35)$$

with \mathcal{R} being the p_T range reported by experiments. Similarly, we define the absolute percentage of deviation of the p_T average by replacing $\langle \mathcal{P}_T \rangle$ with $\langle p_T \rangle$ in Eq. (34). Figure 7 shows our comparison for the first moment and the average of p_T . Notice the agreement between the estimations of the Hagedorn and U fitting functions and the value computed from the experimental data.

B. Variance of the transverse momentum

The variance of the TMD is immediately calculated as $\text{var}(\mathcal{P}_T) = \langle \mathcal{P}_T^2 \rangle - \langle \mathcal{P}_T \rangle^2$ for the three approaches

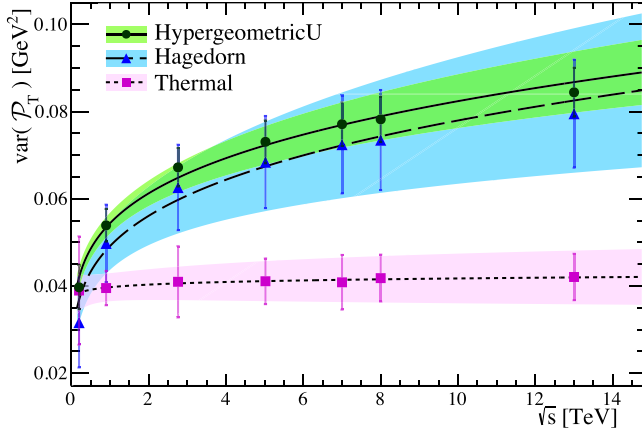


FIG. 8. Variance of the TMD as a function of the center-of-mass energy for minimum bias pp collisions for the three different approaches. Lines, figures, and colors are the same as in Fig. 5.

considered:

$$\text{var}_{\text{th}}(\mathcal{P}_T) = T_{\text{th}}^2, \quad (36a)$$

$$\text{var}_{\text{Hag}}(\mathcal{P}_T) = \frac{m^2(m+1)}{(m-3)(m-2)^2} T_{\text{Hag}}^2, \quad (36b)$$

$$\text{var}_U(\mathcal{P}_T) = F(q)T_U^2, \quad (36c)$$

with $F(q) = \frac{2(q-1)}{3-2q} \left(\frac{\Gamma(\frac{1}{q-1})}{\Gamma(\frac{1}{q-1}-\frac{1}{2})} \right)^2 - \left(\frac{4-2q}{5-3q} \right)^2$.

The dependences of q , σ , m , p_0 , and T_{th} with the center-of-mass energy are considered in the Eqs. (36) via Eqs. (18), (19), and (20). Figure 8 shows the variance of the TMD as a function of the center-of-mass energy of minimum bias pp collisions for the three different approaches with their corresponding estimations. Similarly to the $\langle \mathcal{P}_T \rangle$ case, the variance is proportional to the squared thermal temperature in the three cases, given by combinations of the exponent parameters of Hagedorn and U fitting functions. The expressions (36) reveal that the widths of the TMD for the Hagedorn and U functions are larger than that of the thermal function, as seen in Fig. 8.

It is worth mentioning that the computation of $\langle p_T^2 \rangle$ is crucial for the phenomenology calibration of some models, such as the color string percolation model (CSPM) [19,20]. In this model, the average of p_T^2 and the multiplicity of the produced charged particles comes from the color interaction between strings. It has been shown that overlapping the color string leads to a suppression of the color field. An immediate consequence is that the clusters of strings produce fewer particles per string but enhance their transverse momentum. Finally, the estimation of $\langle p_T^2 \rangle$ allows the CSPM to be fine-tuned with the experimental data [45–48].

C. Kurtosis of the TMD

The kurtosis is calculated as usual:

$$\tilde{\mu} = \frac{\langle \mathcal{P}_T \rangle^4}{[\text{var}(\mathcal{P}_T)]^2} \left[\frac{\langle \mathcal{P}_T^4 \rangle}{\langle \mathcal{P}_T \rangle^4} - 4 \frac{\langle \mathcal{P}_T^3 \rangle}{\langle \mathcal{P}_T \rangle^3} + 6 \frac{\langle \mathcal{P}_T^2 \rangle}{\langle \mathcal{P}_T \rangle^2} - 3 \right], \quad (37)$$

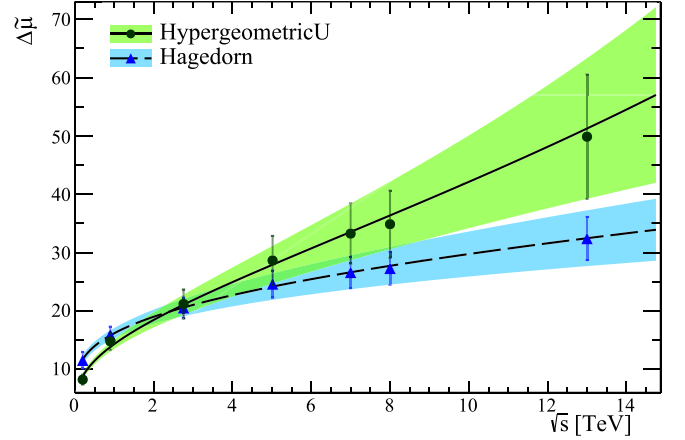


FIG. 9. Excess of kurtosis calculated with respect to the thermal distribution as a function of the center-of-mass energy for pp collisions. Lines, figures, and colors for the Hagedorn and U fitting functions are the same as in Fig. 5.

which for the thermal case is exactly 9. For the Hagedorn and U functions, we substitute the needed moments from Eqs. (24) and (29) into the Eq. (37). We also consider the dependence of the fitting parameters on the center-of-mass energy, as discussed in Sec. III. Figure 9 shows the excess of kurtosis, defined as $\Delta\tilde{\mu} = \tilde{\mu} - 9$, for the Hagedorn and hypergeometric U fitting functions.

Notice that both the Hagedorn and U fitting functions reveal that their descriptions contain more information about heavy tails since $\Delta\tilde{\mu} > 0$. Furthermore, $\Delta\tilde{\mu}$ increases as the center-of-mass energy rises. In fact, the q -Gaussian fluctuations induce a TMD with more information in the tail than the Hagedorn function, despite the latter being a QCD based function. Remarkable, the U function encodes information related to both soft and hard scales.

V. SHANNON ENTROPY AND HEAT CAPACITY

Let us delve into a fundamental concept in information theory, the Shannon entropy. It provides a way to quantify the uncertainty and information of the TMD [49]. This observable can shed light on the characteristics of the final state particles of collision systems. Since the temperature-like parameter T is extracted from the TMD in each approach, the natural way of computing the Shannon entropy is by considering the normalized TMD as the probability density function of the random variable p_T , as is usually done in the generalized ensemble theory [50,51]. Then, the Shannon entropy is computed as [49]

$$\mathcal{H} = - \int_0^\infty (\text{TMD}/I_0) \ln [\text{TMD}/I_0] dp_T, \quad (38)$$

where I_0 is the normalization constant given by Eq. (23).

The Shannon entropy (38) can be expressed in terms of elementary functions for the thermal and Hagedorn fitting

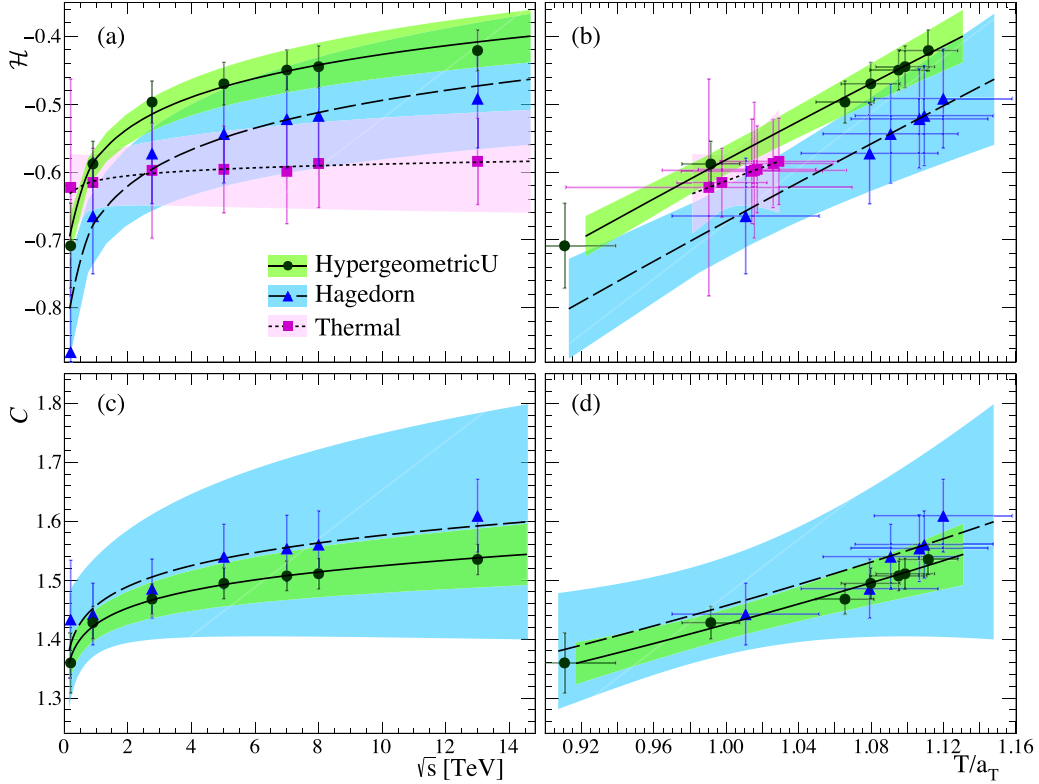


FIG. 10. Shannon entropy dependence on the (a) center-of-mass energy and (b) temperature. Heat capacity as a function of the (c) center-of-mass energy and (d) temperature scaled by a_T . The shaded regions correspond to the uncertainty propagation of the corresponding equations. Lines, figures, and colors for the thermal, Hagedorn, and U fitting functions are the same as in Fig. 5.

functions. For these cases, we obtain

$$\mathcal{H}_{\text{th}} = 1 + \ln(T_{\text{th}}). \quad (39a)$$

$$\mathcal{H}_{\text{Hag}} = \frac{m}{m-1} + \ln\left(\frac{m}{m-1}\right) + \ln(T_{\text{Hag}}), \quad (39b)$$

respectively.

On the other hand, the Shannon entropy of the confluent hypergeometric function is explicitly given by

$$\mathcal{H}_U = - \int_0^\infty (U(a, b, z)/I_0) \ln [U(a, b, z)/I_0] dp_T, \quad (40)$$

with

$$I_0 = \frac{\sigma}{(2-q)\Gamma(a)} \sqrt{\frac{q-1}{2}}, \quad (41)$$

which can be rewritten as

$$\mathcal{H} = \ln(I_0) + \frac{\mathcal{H}_1}{I_0}, \quad (42)$$

where

$$\mathcal{H}_1 = - \int_0^\infty U(a, b, z) \ln [U(a, b, z)] dp_T. \quad (43)$$

As far as we know, Eq. (43) cannot be solved analytically. Then, we computed \mathcal{H}_1 by using numerical methods. Figure 10 shows our estimations of the Shannon entropy for

minimum bias pp collisions as a function of the center-of-mass energy and the corresponding temperature for each approach.

We also compute the heat capacity using its thermodynamic definition [52]

$$C = T \frac{d\mathcal{H}}{dT}. \quad (44)$$

In this context, Eq. (44) is a measure of how much “heat” is necessary to “warm” the TMD. “Heating” the TMD must be understood as a global change of the TMD shape, flattening the soft part together with an enhancement of the TMD tail.

To compute Eq. (44), we must take into account that the fitting parameters may depend on the temperature. In these cases, the computation of the heat capacity must be done using the chain rule. In particular, for the thermal case, we found $C_{\text{th}} = 1$. In the case of the Hagedorn fitting function, the heat capacity is given by

$$C_{\text{Hag}} = 1 + T_{\text{Hag}} \frac{1-2m}{m(m-1)^2} \frac{dm}{dT_{\text{Hag}}}, \quad (45)$$

where the derivative dm/dT_{Hag} for minimum bias pp collisions is computed through Eq. (19a) and using the inverse relation of the temperature with the center-of-mass energy in

Eq. (20), which reads

$$\frac{dm}{dT_{\text{Hag}}} = \frac{c_m m(T_{\text{Hag}})}{c_T T_{\text{Hag}}}. \quad (46)$$

Plugging Eq. (46) into (45), the heat capacity is

$$C_{\text{Hag}} = 1 + \frac{c_m [1 - 2m(T_{\text{Hag}})]}{c_T [m(T_{\text{Hag}}) - 1]^2}, \quad (47)$$

with $m(T_{\text{Hag}}) = a_m (T_{\text{Hag}}/a_T)^{c_m/c_T}$.

On the other hand, for the calculation of the heat capacity of the confluent hypergeometric U function, we start replacing σ in favor of T_U through Eq. (10). Thus, the normalization constant I_0 and the z parameter [see (7)] in the third argument

of the U functions are rewritten as follows:

$$I_0 = \sqrt{\pi} \frac{(q-1)\Gamma(a+\frac{1}{2})}{(2-q)\Gamma(a)} T_U = I_{0q}(q) T_U, \quad (48)$$

$$z = \left(\frac{\Gamma(a)}{\Gamma(a+\frac{1}{2})} \right)^2 \frac{p_T^2}{2T_U^2}. \quad (49)$$

Therefore, the heat capacity for the U fitting function is

$$C_U = \left(1 - \frac{\mathcal{H}_1}{I_0} \right) \left(1 + T_U \frac{I'_{0q}}{I_{0q}} \frac{dq}{dT_U} \right) - \frac{T_U}{I_0} \int_0^\infty (\ln U + 1) \frac{dU}{dT_U} dp_T. \quad (50)$$

In Eq. (50), the remaining integral is

$$\begin{aligned} \int_0^\infty (\ln U + 1) \frac{dU}{dT_U} dp_T &= \frac{\sqrt{2\pi} a (q-2) \Gamma(a+\frac{1}{2})}{(a-\frac{1}{2})^2 (q-3) \Gamma(a)} \left\{ \left(\frac{\Gamma(a+\frac{1}{2})}{\Gamma(a)} \right)^2 - \left(a + \frac{1}{2} \right)^2 \left[\psi^{(0)}\left(a + \frac{1}{2} \right) - \psi^{(0)}(a) \right] T_U \frac{dq}{dT_U} \right\} \\ &\quad - \left(a + \frac{1}{2} \right) \frac{dq}{dT_U} \int_0^\infty [\ln U(a, 1/2, z) + 1] U^{(1,0,0)}(a, 1/2, z) dp_T + \frac{a}{T_U^2} \left(\frac{\Gamma(a)}{\Gamma(a+\frac{1}{2})} \right)^2 \\ &\quad \times \left\{ \frac{1}{T_U} - \left[\psi^{(0)}\left(a + \frac{1}{2} \right) - \psi^{(0)}(a) \right] \frac{dq}{dT_U} \right\} \int_0^\infty p_T^2 U(a+1, 3/2, z) \ln U(a, 1/2, z) dp_T, \quad (51) \end{aligned}$$

where $\psi^{(0)}(x)$ is the zeroth-order polygamma function. We also added the superscript to the U function to denote its first derivative with respect to the first argument. Notice that there are two remaining integrals, which are done by means of numerical methods. Similarly to the case of the Hagedorn fitting function, q is expressed as a power law as a function of T_U , i.e., $q(T_U) = a_q (T_U/a_T)^{c_q/c_T}$, and its derivative with respect to the temperature is

$$\frac{dq}{dT_U} = \frac{c_q}{c_T} \frac{q(T_U)}{T_U}. \quad (52)$$

The heat capacities of the three different schemes as a function of the center-of-mass energy and the temperature are plotted in Fig. 10.

VI. CONCLUSIONS

In this work, we discussed the statistics of three different fitting functions that describe the TMD data, namely, the thermal p_T -exponential, the confluent hypergeometric, and the Hagedorn functions. The first two arise from the string tension fluctuation in the QCD color string picture; meanwhile, the last is a power law inspired by the foundations of QCD. All of them predict a temperature parameter at the low p_T regime.

The temperature estimated for minimum bias pp collisions as a function of the center-of-mass energies reflects the physical motivation of the different approaches. The thermal distribution adequately describes the soft part because it assumes an exponential decay (similar to a Boltzmann dis-

tribution), resulting in overestimating the temperature for the complete TMD. In contrast, the power law proposed by Hagedorn establishes a description of the hard processes, leading to a power law tail of the spectrum. This means that the thermal temperature may not precisely incorporate the soft part of the TMD. In fact, Hagedorn suggests that their fit must be performed in the p_T interval from 0.3 to 10 GeV [11]. On the other hand, we must emphasize that the confluent hypergeometric U adequately combines the information of the soft and hard scales to predict the temperature.

We also discussed the statistics of the normalized TMD by computing the moments of the distribution and, thus, the variance and kurtosis for the three different approaches. This analysis lets us distinguish the particularities of each fitting function. For example, the Hagedorn and U functions reveal more dispersion than the thermal one because of the information coming from the TMD tail. In all cases, we found an increasing trend of the first moment and variance with the center-of-mass energy, as seen in Figs. 6 and 8. Moreover, the power law tail absence in the thermal distribution leads to a constant kurtosis, which was taken as a reference to measure the excess of kurtosis in the Hagedorn and U functions, both increasing as the center-of-mass energy rises, highlighting that the U grows more substantially (see Fig. 9). This means the TMD derived from the q -Gaussian string tension fluctuations contains more information in the tail than the Hagedorn approach. This is important because the U fitting function adequately reproduces the power law behavior associated with the QCD hard processes from the color string picture.

In addition, we compare the average of the transverse momentum estimated from the fitting function and that computed from the experimental data. It was found that the Hagedorn and U functions precisely reproduce the value of $\langle p_T \rangle^{\text{hist}}$, but the predictions of the thermal distribution considerably deviate (15%–25%).

Other observables that we computed are the Shannon entropy and the heat capacity. The Shannon entropy increases as the center-of-mass energy grows. This is consistent with the TMD variance, which exhibits a similar behavior. This happens because the probability of observing particles with high p_T rises with an increment on the center-of-mass energy. Then, the TMD suffers a global widening and an enhancement of its tail. Moreover, we observed sharp differences between the entropy computed for the Hagedorn and hypergeometric confluent U functions. These subtle deviations may come from the shape of the TMD at very low p_T , which can be inferred from the temperature estimated by each model.

Moreover, the computation of the heat capacity for the thermal fitting function reveals that the system does not change its requirements to *heat up*. From a classical thermodynamics point of view, this means that collision systems described by a thermal distribution resemble an ideal gas of monoatomic (or rigid diatomic) molecules. In contrast, for the Hagedorn and U functions, the heat capacity grows as the temperature does, similar to a thermodynamic system that can manifest other degrees of freedom when heating. This implies that, to *heat up* the collision system, it is necessary to reach in-

creasingly higher center-of-mass energies. This is a direct consequence of the TMD tail, since it is required to *heat* not only the thermal part but also the hard one for the discussed minimum bias pp collisions. From our results, we infer that the higher the TMD temperature, the more energetic collision is required. This observation is consistent with the analysis of the experimental data of the temperature saturation as a function of the center-of-mass energy (see Fig. 5).

This work can be extended in several ways. For instance, it would be interesting to analyze the TMD and compute the Shannon entropy and heat capacity of pp collisions as a function of the multiplicity, heavy ion collisions, production of identified particles, and other processes. Part of these results are currently under discussion, and we will report our findings in a future paper.

ACKNOWLEDGMENTS

This work has been funded by the projects PID2020-119632GB-I00 of the Spanish Research Agency, Centro Singular de Galicia 2019–2022 of Xunta de Galicia and the ERDF of the European Union. This work was funded by Consejo Nacional de Humanidades, Ciencias y Tecnologías (CONAHCYT-México) under Project No. CF-2019/2042, graduate fellowship Grant No. 1140160, and postdoctoral fellowship Grants No. 645654 and No. 289198. J.R.A.G. acknowledges financial support from Vicerrectoría de Investigación y Estudios de Posgrado (VIEP-BUAP).

-
- [1] J. D. Bjorken, *Phys. Rev. D* **27**, 140 (1983).
- [2] R. Vogt, in *Ultrarelativistic Heavy-Ion Collisions*, edited by R. Vogt (Elsevier Science, Amsterdam, 2007), pp. 221–278
- [3] F. Becattini, *Z. Phys. C* **69**, 485 (1995).
- [4] F. Becattini, *J. Phys. G* **23**, 1933 (1997).
- [5] A. Bialas, *Phys. Lett. B* **747**, 190 (2015).
- [6] X. Feal, C. Pajares, and R. A. Vazquez, *Phys. Rev. C* **104**, 044904 (2021).
- [7] P. Braun-Munzinger, J. Stachel, J. Wessels, and N. Xu, *Phys. Lett. B* **344**, 43 (1995).
- [8] P. Braun-Munzinger, J. Stachel, and C. Wetterich, *Phys. Lett. B* **596**, 61 (2004).
- [9] R. Hagedorn, *Nuovo Cimento Suppl.* **3**, 147 (1965).
- [10] J. Rafelski, Thermodynamics of Distinguishable Particles: A Key to High-Energy Strong Interactions? in *Melting Hadrons, Boiling Quarks - From Hagedorn Temperature to Ultra-Relativistic Heavy-Ion Collisions at CERN: With a Tribute to Rolf Hagedorn* (Springer, Cham, 2016), pp. 183–222.
- [11] R. Hagedorn, *Riv. Nuovo Cimento* **6**, 1 (1983).
- [12] G. Wilk and Z. Włodarczyk, *Phys. Rev. Lett.* **84**, 2770 (2000).
- [13] G. Bíró, G. G. Barnaföldi, and T. S. Bíró, *J. Phys. G: Nucl. Part. Phys.* **47**, 105002 (2020).
- [14] K. Saraswat, P. Shukla, and V. Singh, *J. Phys. Commun.* **2**, 035003 (2018).
- [15] B. Andersson, *The Lund Model* (Cambridge University Press, Cambridge, 1998).
- [16] J. Schwinger, *Phys. Rev.* **128**, 2425 (1962).
- [17] A. Bialas, *Phys. Lett. B* **466**, 301 (1999).
- [18] J. Dias de Deus and C. Pajares, *Phys. Lett. B* **642**, 455 (2006).
- [19] M. A. Braun, J. Dias de Deus, A. S. Hirsch, C. Pajares, R. P. Scharenberg, and B. K. Srivastava, *Phys. Rep.* **599**, 1 (2015).
- [20] I. Bautista, C. Pajares, and J. E. Ramírez, *Rev. Mex. Fís.* **65**, 197 (2019).
- [21] C. Pajares and J. E. Ramírez, *Eur. Phys. J. A* **59**, 250 (2023).
- [22] J. R. Alvarado García, D. Rosales Herrera, P. Fierro, J. E. Ramírez, A. Fernández Téllez, and C. Pajares, *J. Phys. G: Nucl. Part. Phys.* **50**, 125105 (2023).
- [23] A. Bialas and W. Czyz, *Nucl. Phys. B* **267**, 242 (1986).
- [24] C.-Y. Wong, *Introduction to High-Energy Heavy-Ion Collisions* (World Scientific, Singapore, 1994).
- [25] B. Andersson, G. Gustafson, G. Ingelman, and T. Sjostrand, *Phys. Rep.* **97**, 31 (1983).
- [26] R. Kubo, M. Toda, and N. Hashitsume, *Statistical Physics II: Nonequilibrium Statistical Mechanics*, Springer Series in Solid-State Sciences, Vol. 31 (Springer, Berlin, 2012).
- [27] A. A. Budini, *Phys. Rev. E* **91**, 052113 (2015).
- [28] A. A. Budini, *Phys. Rev. E* **86**, 011109 (2012).
- [29] L. J. Slater, in *Handbook of Mathematical Functions with Formulas, Graphs, and Mathematical Tables*, edited by M. Abramowitz and I. A. Stegun (National Bureau of Standards, Washington, DC, 1972), Chap. 13, pp. 503–536.
- [30] J. Cleymans and D. Worku, *Eur. Phys. J. A* **48**, 160 (2012).
- [31] A. S. Parvan and T. Bhattacharyya, *Eur. Phys. J. A* **56**, 72 (2020).
- [32] D. Sahu and R. Sahoo, *Physics* **3**, 207 (2021).

- [33] J. Tao, W. Wu, M. Wang, H. Zheng, W. Zhang, L. Zhu, and A. Bonasera, *Particles* **5**, 146 (2022).
- [34] STAR Collaboration, *Phys. Rev. C* **75**, 064901 (2007).
- [35] ALICE Collaboration, *Eur. Phys. J. C* **71**, 1655 (2011).
- [36] V. Khachatryan *et al.* (CMS Collaboration), *J. High Energy Phys.* **05** (2011) 064..
- [37] A. A. Bylinkin, D. E. Kharzeev, and A. A. Rostovtsev, *Int. J. Mod. Phys. E* **23**, 1450083 (2014).
- [38] A. Bylinkin and A. Rostovtsev, *Nucl. Phys. B* **888**, 65 (2014).
- [39] O. K. Baker and D. E. Kharzeev, *Phys. Rev. D* **98**, 054007 (2018).
- [40] X. Feal, C. Pajares, and R. A. Vazquez, *Phys. Rev. C* **99**, 015205 (2019).
- [41] R. Bellwied, *J. Phys.: Conf. Ser.* **1070**, 012001 (2018).
- [42] J. Adams *et al.* (STAR Collaboration), *Phys. Rev. Lett.* **91**, 172302 (2003).
- [43] K. Aamodt *et al.* (ALICE Collaboration), *Phys. Lett. B* **693**, 53 (2010).
- [44] S. Acharya *et al.* (ALICE Collaboration), *Phys. Lett. B* **845**, 138110 (2023).
- [45] J. E. Ramírez and C. Pajares, *Phys. Rev. E* **100**, 022123 (2019).
- [46] J. E. Ramírez, B. Díaz, and C. Pajares, *Phys. Rev. D* **103**, 094029 (2021).
- [47] J. C. Texca García, D. Rosales Herrera, J. E. Ramírez, A. Fernández Téllez, and C. Pajares, *Phys. Rev. D* **106**, L031503 (2022).
- [48] J. R. Alvarado García, D. Rosales Herrera, A. Fernández Téllez, B. Díaz, and J. E. Ramírez, *Universe* **9**, 291 (2023).
- [49] C. E. Shannon, *Bell Syst. Tech. J* **27**, 379 (1948).
- [50] R. K. Niven and B. Andresen, in *Complex Physical, Biophysical and Econophysical Systems* (World Scientific, Singapore, 2010), pp. 283–317.
- [51] T. Langen, S. Erne, R. Geiger, B. Rauer, T. Schweigler, M. Kuhnert, W. Rohringer, I. E. Mazets, T. Gasenzer, and J. Schmiedmayer, *Science* **348**, 207 (2015).
- [52] D. Mandal, *Phys. Rev. E* **88**, 062135 (2013).